Archives of Virology (2023) 168:82
https://doi.org/10.1007/s00705-022-05646-w

ORIGINAL ARTICLE

Comparative pathogenic potential of avian influenza H7N3 viruses isolated from wild birds in Egypt and their sensitivity to commercial antiviral drugs

Ahmed E. Kayed[1] · Omnia Kutkat[1] · Ahmed Kandeil[1] · Yassmin Moatasim[1] · Ahmed El Taweel[1] · Mohamed El Sayes[1] · Rabeh El-Shesheny[1] · Basma Emad Aboulhoda[2] · Nourtan F. Abdeltawab[3] · Ghazi Kayali[4] · Mohamed A. Ali[1] · Mohammed A. Ramadan[3]

Received: 28 June 2022 / Accepted: 3 November 2022 / Published online: 9 February 2023

Abstract

Active surveillance and studying the virological features of avian-origin influenza viruses are essential for early warning and preparedness for the next potential pandemic. During our active surveillance of avian influenza viruses in wild birds in Egypt in the period 2014-2017, multiple reassortant low-pathogenic avian influenza H7N3 viruses were isolated. In this study, we investigated and compared the infectivity, pathogenicity, and transmission of four different constellation forms of Egyptian H7N3 viruses in chickens and mice and assessed the sensitivity of these viruses to different commercial antiviral drugs *in vitro*. Considerable variation in virus pathogenicity was observed in mice infected with different H7N3 viruses. The mortality rate ranged from 20 to 100% in infected mice. Infected chickens showed only ocular clinical signs at three days postinfection as well as systemic viral infection in different organs. Efficient virus replication and transmission in chickens was observed within each group, indicating that these subtypes can spread easily from wild birds to poultry without prior adaptation. Mutations in the viral proteins associated with antiviral drug resistance were not detected, and all strains were sensitive to the antiviral drugs tested. In conclusion, all of the viruses studied had the ability to infect mice and chickens. H7N3 viruses circulating among wild birds in Egypt could threaten poultry production and public health.

Introduction

Each year, avian influenza viruses (AIVs) cause regional outbreaks in birds in various parts of the world, and they sometimes give rise to influenza viruses that cause human influenza pandemics [27]. These pandemics usually occur due to antigenic shifts caused by an exchange of viral genes among human-, swine-, and wild- and/or domestic-bird-adapted strains [25]. Wild birds are frequently exposed to AIV, and wild aquatic birds are considered the primary virus reservoir [38]. Influenza viruses with more than 80 different combinations of HA and NA subtypes have been isolated from wild birds [28]. Asymptomatic transmission of AIVs among wild birds in particular increases the potential of AIVs to spread between countries or even continents during their annual migration [17].

Anseriforms (waterfowl) carry a distinct pool of influenza viruses [19, 45], and H7 AIV is one of the frequent subtypes identified in migratory waterfowl [2, 11]. Low-pathogenic avian influenza virus (LPAIV) subtype H7N3 was one of the strains most frequently detected during our

Handling Editor: Sheela Ramamoorthy.

✉ Ghazi Kayali
ghazi@human-link.org

✉ Mohamed A. Ali
Mohamed.Ali@human-link.org

✉ Mohammed A. Ramadan
mohamed.abdelhalim@pharma.cu.edu.eg

[1] Environmental Research Division, Centre of Scientific Excellence for Influenza Viruses, National Research Centre, Giza 12622, Egypt

[2] Department of Anatomy and Embryology, Faculty of Medicine, Cairo University, Cairo 12613, Egypt

[3] Department of Microbiology and Immunology, Faculty of Pharmacy, Cairo University, Cairo 12613, Egypt

[4] Human Link DMCC, Dubai, United Arab Emirates

previous surveillance study of AIVs in wild birds in Egypt [16]. Infection with LPAIV H7 and H5 subtypes in waterfowl is asymptomatic, and the birds can transmit the virus over long distances during their annual migration and spill the infection over into domestic poultry [21].

During infection of domestic galliforms with LPAIV H5 and H7 subtypes, the virus can potentially evolve into a highly pathogenic avian influenza virus (HPAIV) by insertion or substitution of basic amino acids at the HA0 cleavage site [3, 32, 46]. Alternatively, coinfection with more than one AIV can result in recombination of the HA gene with other viral genes of non-homologous viruses, giving rise to a more pathogenic virus that causes severe systemic disease and mortality [39].

H7 viruses occasionally spill over from wild birds into domestic poultry, causing economic losses in poultry production and sporadic infections in humans [18]. The first isolation of H7N3 viruses was reported in Britain in 1963, during an outbreak on a turkey farm, and in 1994, Australia and Pakistan were affected by HPAI variants [1]. Other outbreaks of H7N3 HPAIV in poultry were reported in China in 2002 [33], Canada in 2004 [14] and 2007 [6], and Chile in 2002 [39]. In 2020, an outbreak of H7N3 LPAIV occurred on a turkey farm in the USA, and the virus was found to be closely related to wild-bird isolates of North American lineage [44].

Genetic analysis of Egyptian H7N3 viruses isolated during our active surveillance study of wild birds during the period 2014-2016 indicated the presence of four different H7N3 viruses with different genome constellations [16]. Here, we investigated the replication and pathogenicity of these viruses in avian and mammalian hosts as well as their sensitivity *in vitro* to different commercial antivirals, including oseltamivir and zanamivir (neuraminidase inhibitors) [22], amantadine (an M2 blocker) [41], and favipiravir (an RdRp inhibitor) [13].

Materials and methods

Viruses

The LPAIVs used in this study were isolated through routine AIV surveillance of wild birds [16]. All four viruses – A/teal/Egypt/MB.D125OP/2015, A/teal/Egypt/MB.D128OP/2015, A/teal/Egypt/MB.D487OP/2016, and A/northern shoveler/Egypt/MB.D690OP/2016 (hereafter abbreviated as 125OP, 128OP, 487OP, and 690OP) – were isolated from Damietta governorate in the same migration season (at the end of 2015 and beginning of 2016). Full genome sequencing was conducted [10], and the sequences of the segments were subjected to BLAST analysis on the Global Initiative on Sharing All Influenza Data (GISAID) platform (Fig. 1). Sequences are available in the GenBank database under the accession numbers listed in Table 1. The viruses were purified by plaque assay [12] and then propagated in specific-pathogen-free (SPF) eggs. Aliquots were stored at -80 °C and titrated using egg infectious dose 50 (EID_{50}) and plaque assays [15, 31].

Pathogenicity of the virus isolates in SPF chickens

Twelve 12 30-day-old SPF chickens obtained from the SPF Egg Production Farm, Koum Osheim, El-Fayoum, Egypt, were infected with 10^6 EID_{50} of each virus in a volume of 200 µl via the intraocular and intranasal routes. Chickens were kept in class II isolator cages and monitored daily for mortality and any clinical signs for 10 days postinfection (dpi). After 12 hours of infection, five naïve SPF chickens were placed in the same cage to assess the ability of the infected chickens to infect members of the naïve group. Oropharyngeal and cloacal swabs were collected from three randomly selected chickens from the inoculated group, while all of the chickens in the naïve group were swabbed at 3, 5, 7, and 10 dpi. Swabs were stored in transport medium at -80 °C. Three chickens from the infected group were selected randomly and euthanized, and a postmortem examination was performed at 7 dpi. Brain, lung, trachea, liver, spleen, intestine, and bursa of Fabricius were collected and kept at -80 ºC.

Pathogenicity of the isolated viruses in C57BL/6 mice

We investigated the use of mice as a mammalian model for H7N3 infection. Eight 21-day-old female C57BL/6 mice obtained from the animal house of the National Research Center, Cairo, Egypt, were infected intranasally with 10^6 EID_{50} of each virus in a volume of 20 µl. The mice were kept in class II isolator cages and monitored daily for mortality, body weight loss, and any clinical signs for 10 dpi. Serum samples and nasal washes obtained by washing the nasal passages of the mice with 10 µl of sterile PBS were collected from three randomly selected mice at 3, 5, and 7 dpi and then kept at -80 °C.

Organ homogenization and EID_{50} titration

The collected organs were weighed and aliquoted, and 0.1 g of each organ was suspended in 900 µl of PBS (dilution 10^{-1}) and then homogenized twice for 5 min using a TissueLyser LT (QIAGEN, Hilden, Germany). All organ suspensions were centrifuged at 4000 rpm to remove cell debris and serially diluted (10^{-2}, 10^{-3}, and 10^{-4}) in PBS. The amount of virus present in the swabs and homogenized organs was quantified using an EID_{50} assay. The prepared dilutions were

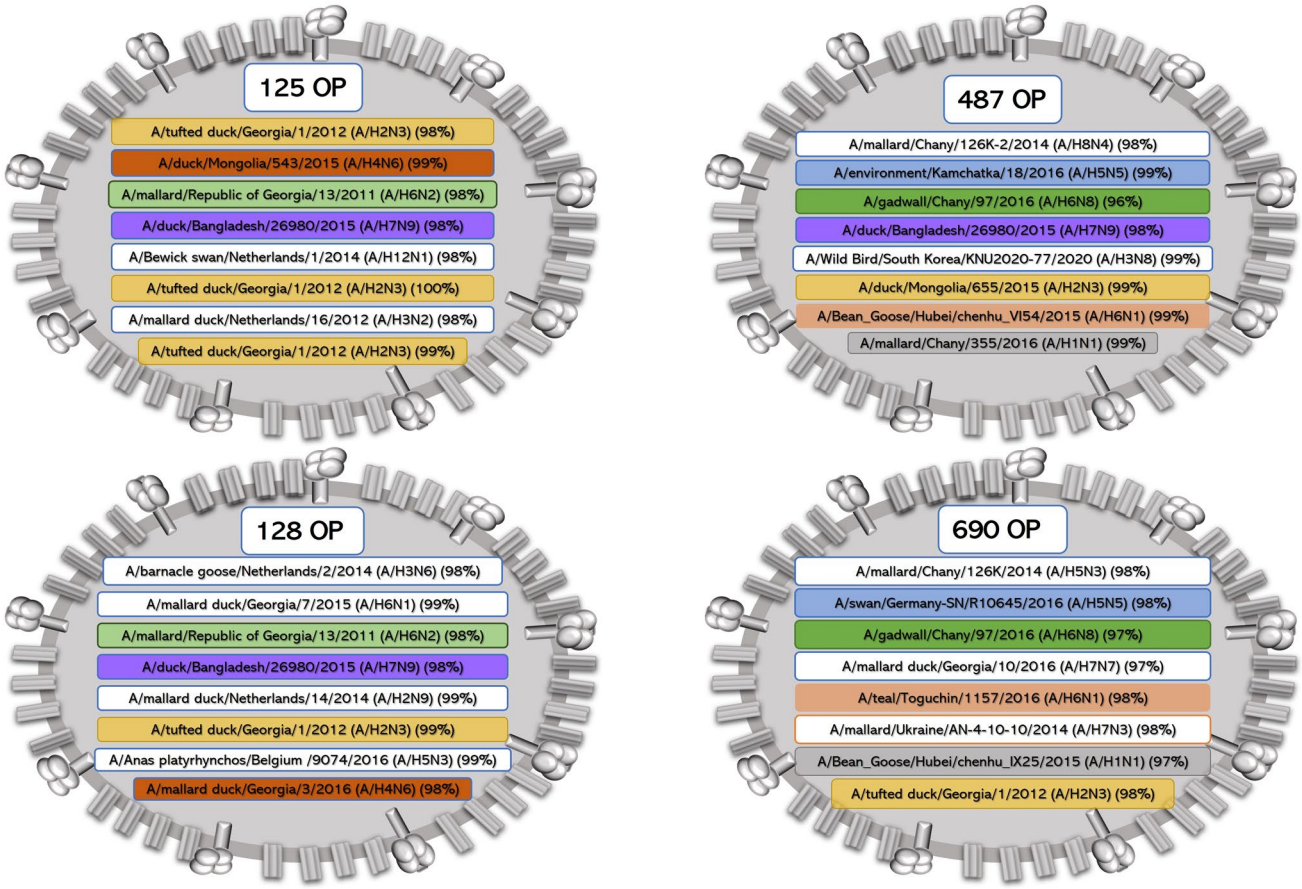

Fig. 1 Genetic constellation of the four detected H7N3 viruses. Similar segments are shown with the same color.

Table 1 Sequence accession numbers for the four H7N3 viruses

	NA	NP	PB2	PB1	HA	PA	MP	NS
A/teal/Egypt/MB-D-125OP/2015	MN208018	MN208019	MN208020	MN208021	MN208022	MN208023	MN208024	MN208025
A/teal/Egypt/MB-D-128OP/2015	OP208841,	OP208842	OP208843	OP226138	OP208839	OP226137	OP208840	OP226136
A/teal/Egypt/MB-D-487OP/2016	MN208010	MN208011	MN208012	MN208013	MN208014	MN208015	MN208016	MN208017
A/northern shoveler/Egypt/MB-D-690OP/2016	MN207997	MN207998	MN207999	MN208000	MN208001	MN208002	MN208003	MN208004

inoculated into SPF eggs in triplicate. Inoculated eggs were incubated at 37 ℃ and candled daily for up to 72 h. Allantoic fluid was collected from dead embryos and from live eggs 72 h after infection and tested by hemagglutination assay [23].

Hemagglutination inhibition (HI) assay

The collected sera from mice were treated with receptor-destroying enzyme (RDE) (Denka Seiken, Tokyo, Japan). Three volumes of RDE were added to one volume of serum and incubated overnight at 37 ℃. In the morning, the serum/RDE mixture was heated at 56 °C for 30 min to inactivate the enzyme [42]. Hemoadsorption of RDE-treated sera was then performed to remove any nonspecific agglutinins by adding 5% of packed chicken RBCs to each sample. The serum-RBC mixture was mixed thoroughly and incubated at 4 °C for one hour.

In a microtiter plate, 25 µl of PBS was added to all but the first row of wells, and 50 µl of treated serum was added to the first row, and serial dilution was performed by sequentially transferring a volume of 25 µl. All sera were tested with the four forms of LPAI H7N3 antigens (homologous and heterologous) by adding 25 µl of the antigen and incubation for 30 min. Finally, 50 µl of 0.5% chicken RBCs were

added and incubated for 30 min, and the wells were observed for hemagglutination.

Determination of the half-maximal cytotoxic concentration by MTT assay

The half-maximal cytotoxic concentration (CC_{50}) values for oseltamivir, zanamivir, amantadine, favipiravir, and remdesivir were determined using a 3-(4,5-dimethylthiazol-2-yl)-2,5 diphenyltetrazolium bromide (MTT) assay [7]. A 96-well plate was seeded with Madin-Darby canine kidney (MDCK) cells (2.4 × 104 cells/well) and incubated overnight at 37 °C in a 5% CO_2 incubator. The compounds were prepared in twofold serial dilutions in DMEM from 15 mM to 3 µM in a 96-well plate, and MDCK cells were treated with various concentrations of the tested compounds in triplicate. After incubation at 37 °C for 24 h, the cells were washed with 1X PBS balanced salt solution, and 20 µL of MTT solution (5 mg/mL) was added to each well. The cells were then incubated at 37 °C for 3 h to allow crystals of violet formazan to be formed. The resulting crystals were dissolved in dimethyl sulfoxide (Sigma-Aldrich, St. Louis, MO, USA), and the absorbance was measured at 540 nm, with 620 nm as a reference wavelength, using a multi-well plate reader. CC_{50} values were calculated by nonlinear regression analysis in GraphPad Prism software version 5.01 (GraphPad, San Diego, CA, USA).

Measurement of antiviral activity by crystal violet assay

The 50% inhibitory concentration (IC_{50}) of the compounds was determined by crystal violet assay [24]. MDCK cells in complete growth medium consisting of DMEM, 5% fetal bovine serum (FBS; Gibco, Waltham, MA, USA), and 2% antibiotic-antimycotic mixture (Gibco), were cultured in 96-well plates (2.4×10^4 cells/well) at 37 °C with 5% CO_2. After 24 h, each drug was serially diluted twofold in infection medium (DMEM containing 4% bovine serum albumin [BSA], 2% antibiotic-antimycotic mixture, and 0.5 µg of TPCK-treated trypsin per mL) in a separate U-shaped 96-well plate to reach a volume of 100 µL in each well. Then, 100 $TCID_{50}$ of each virus in a volume of 100 µL was added to each well. In parallel, untreated virus control and cell control wells were included in each plate. After incubation for 72 h at 37 °C with 5% CO_2, the cells were fixed using 10% formalin and incubated for at least 2 h at room temperature. The fixed cells were washed three times with water, and the plate was inverted on filter paper to ensure complete drying. A volume of 50 µL of 0.5% crystal violet solution (0.5 g crystal violet powder [Sigma-Aldrich, Germany], 80 mL of distilled water, and 20 mL of methanol) was added to each well of the plate and incubated for 10 min at room temperature. The plates were washed with water, the crystal violet crystals in each well were dissolved in 180 µL of absolute methanol, and the optical density was measured at 570 nm, with a reference value of 620 nm, using an Anthos Zenyth 200rt plate reader (Anthos Labtec Instruments, Heerhugowaard, The Netherlands). The 50% inhibitory concentration (IC_{50}) for each tested compound was calculated by non-linear regression analysis using GraphPad Prism software (version 5.01).

Histopathological examination

Specimens of the lung, trachea, intestine, liver, and bursa of Fabricius were carefully dissected, fixed in 10% formol saline solution, dehydrated in ascending grades of ethyl alcohol, cleared with xylene, embedded in paraffin, and sliced into 5-µm-thick sections. The sections were then stained with hematoxylin and eosin (H&E) and examined using a Leica light microscope coupled to a Leica digital camera.

Results

Replication and transmission of H7N3 viruses in 4-week-old chickens

Four different genetic constellations of H7N3 viruses – A/teal/Egypt/MB.D125OP/2015, A/teal/Egypt/MB.D128OP/2015, A/teal/Egypt/MB.D487OP/2016, and A/northern shoveler/ Egypt/MB.D690OP/2016 – were detected, and their replication ability and transmissibility in SPF chickens were evaluated. Ocular clinical signs were observed after 1 dpi and lasted until 3 dpi (Fig. 2). No deaths occurred in any of the inoculated or contact groups.

Chickens challenged with 125OP shed virus as early as 3 dpi, and shedding continued until 7 dpi, with the highest rate of shedding at 3 dpi (Table 2). The same pattern was observed in the contact group. Cloacal swabs from both the infected and direct contact groups had higher mean viral titers (infected group, 2.15; direct contact group, 3.2 $\log_{10}$ EID_{50}/ml) than oropharyngeal swabs (infected group, 1.92; direct contact group, 1.98 $\log_{10}$ EID_{50}/ml). The group challenged with 128OP virus showed infection early at 3 dpi, and the infection lasted until 7 dpi, with only one chicken in the direct contact group having a positive oropharyngeal swab at 10 dpi. Cloacal swabs from both the infected and direct contact groups had a higher mean viral titer (infected group, 2.47; direct contact group, 2.76 $\log_{10}$ EID_{50}/ml) than oropharyngeal swabs (infected group, 1.82; direct contact group, 1.57 $\log_{10}$ EID_{50}/ml). Chickens challenged with 487OP showed virus infection early at 3 dpi, and the infection continued until 7 dpi, with only one chicken in the direct contact group positive at 10 dpi.

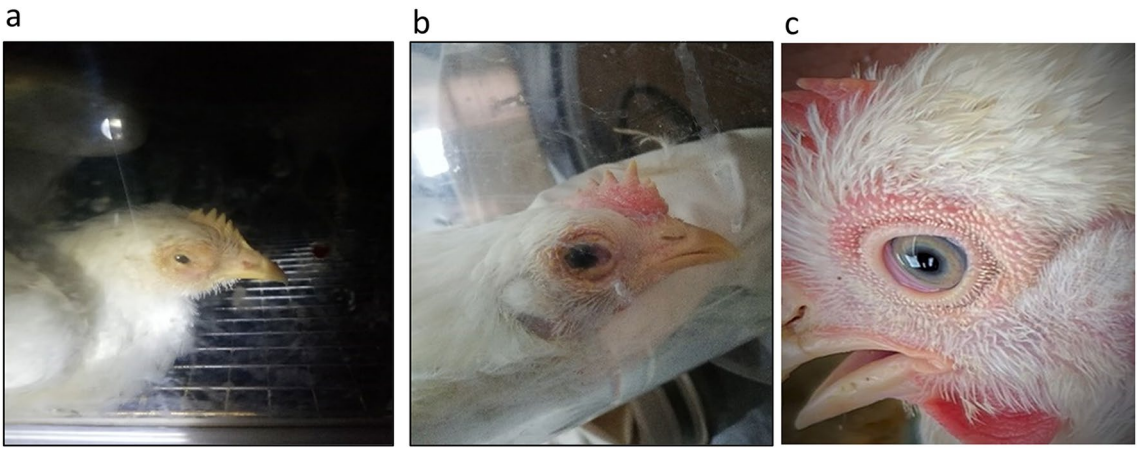

Fig. 2 Representative images showing differences in ocular clinical signs between infected and uninfected chickens. (A and B) Infected chickens at 3 dpi showing ocular clinical signs of irregularly shaped pupils, gray or cloudy eyes, difficulty seeing, and eventually, total blindness. (C) A normal chicken eye

Table 2 Virus shedding in chickens infected with four different LPAI viruses of the H7N3 subtype and contact chicken groups

Group	Sample	Number of infected / inoculated birds (mean virus titer[1] ± SD)			
		Days postinfection			
		3	**5**	**7**	**10**
Inoculated 125OP	OP	3/3 (3.6 ± 0.76)	3/3 (3.1 ± 1.25)	1/3 (1.00 ± 0.00)	0/3 (0.00 ± 0.00)
	C	3/3 (2.5 ± 0.5)	3/3 (3.1 ± 1.15)	2/3 (3.0 ± 1.41)	0/3 (0.0 ± 0.0)
Contact 125OP	OP	5/5 (3.3 ± 0.90)	5/5 (3.4 ± 1.08)	4/5 (1.25 ± 0.50)	0/3 (0.00 ± 0.00)
	C	5/5 (4.9 ± 0.54)	5/5 (4.1 ± 0.41)	5/5 (3.8 ± 0.97)	0/3 (0.0 ± 0.0)
Inoculated 128OP	OP	3/3 (4.0 ± 1.32)	3/3 (2.3 ± 1.04)	1/3 (1.00 ± 0.00)	0/3 (0.00 ± 0.00)
	C	3/3 (3.3 ± 1.89)	3/3 (3.6 ± 0.57)	3/3 (3.0 ± 1.32)	0/3 (0.0 ± 0.0)
Contact 128OP	OP	5/5 (2.2 ± 0.83)	5/5 (2.6 ± 0.65)	3/5 (1.5 ± 0.50)	1/3 (1.00 ± 0.00)
	C	4/5(3.37 ± 1.43)	5/5 (3.9 ± 0.65)	5/5 (3.8 ± 0.75)	0/3 (0.0 ± 0.0)
Inoculated 487OP	OP	3/3 (3.8 ± 0.76)	2/3(2.50 ± 0.70)	2/3 (2.00 ± 0.00)	0/3 (0.00 ± 0.00)
	C	3/3(3.16 ± 1.89)	2/3(2.00 ± 0.00)	2/3 (2.41 ± 1.41)	0/3 (0.0 ± 0.0)
Contact 487OP	OP	5/5 (3.2 ± 1.20)	5/5 (3.5 ± 1.17)	3/5 (1.83 ± 0.28)	1/3 (1.00 ± 0.0)
	C	3/5(2.83 ± 1.60)	5/5 (3.6 ± 1.51)	3/5 (2.33 ± 1.25)	0/3 (0.0 ± 0.0)
Inoculated 690OP	OP	3/3(2.8 ± 0.57)	3/3(2.50 ± 0.86)	1/3 (1.00 ± 0.00)	0/3 (0.00 ± 0.0)
	C	2/3(2.00 ± 0.70)	3/3(3.33 ± 1.04)	1/3 (2.00 ± 0.00)	1/3 (1.0 ± 0.0)
Contact 690OP	OP	5/5 (3.4 ± 0.82)	4/5(3.25 ± 0.86)	1/5 (2.00 ± 0.00)	0/3 (0.00 ± 0.0)
	C	4/5 (2.8 ± 1.31)	5/5 (3.8 ± 0.83)	3/5 (3.5 ± 1.73)	2/3 (1.5 ± 0.70)

[1] $\log_{10}$ EID_{50}/ml

Oropharyngeal swabs in both the infected and direct contact groups had a higher mean viral titer (infected group, 2; direct contact group, 2.38 $\log_{10}$ EID_{50}/ml) than cloacal swabs (infected group, 1.89; direct contact group, 2.19 $\log_{10}$ EID_{50}/ml). The group challenged with 690OP virus showed infection early at 3 dpi, and the infection continued until 7 dpi, with only one chicken in the infected group and two chickens in direct contact group positive at 10 dpi. The cloacal swabs in both the infected and direct contact groups had a higher mean viral titer (infected group, 2; direct contact group, 2.9 $\log_{10}$ EID_{50}/ml) than oropharyngeal swabs (infected group, 1.57; direct contact group, 2.16 $\log_{10}$ EID_{50}/ml).

The viral titers in the collected organs of the inoculated group were determined by the EID_{50} method (Table 3) at 3 and 7 dpi. All of the viruses were found in the lung, trachea, intestine, bursa, and brain after 3 dpi, while the levels of virus in the liver and spleen were low. At 7 dpi, the level of 690OP was low propagation in all organs.

Table 3 Viral titers in organs of SPF chickens challenged with four H7N3 variants

Virus	DPI	Number of infected / inoculated birds (mean virus titer[1] ± SD)						
		Lung	Trachea	Intestine	Liver	Spleen	Bursa	Brain
125OP	3	3/3 (2.5 ± 0.86)	3/3 (1.6 ± 0.76)	3/3 (2.5 ± 0.5)	1/3 (3 ± 0.0)	1/3 (3 ± 0.0)	3/3 (3.33 ± 0.28)	3/3 (2.1 ± 1.04)
	7	1/3 (2.0 ± 0.0)	1/3 (1.0 ± 0.0)	0/3 (0.0 ± 0.0)	0/3 (0.0 ± 0.0)	1/3 (1.00 ± 0.00)	1/3 (3 ± 0.00)	0/3 (0.0 ± 0.0)
128OP	3	2/3 (2.2 ± 1.76)	2/3 (2.50 ± 1.41)	1/3 (3.0 ± 0.0)	2/3 (2.25 ± 0.35)	1/3 (3.5 ± 0.0)	2/3 (3.0 ± 0.7)	1/3 (2.5 ± 0.0)
	7	0/3 (0.0 ± 0.0)	2/3 (1.25 ± 0.35)	2/3 (3.25 ± 0.35)	0/3 (0.0 ± 0.0)	0/3 (0.0 ± 0.0)	1/3 (3.0 ± 0.0)	0/3 (0.0 ± 0.0)
487OP	3	3/3 (1.66±0.57)	1/3 (2.0 ± 0.0)	3/3 (2.66 ± 0.57)	0/3 (0.0 ± 0.0)	0/3 (0.0 ± 0.0)	3/3 (2.50 ± 1.32)	1/3 (2.5 ± 0.0)
	7	0/3 (0.0 ± 0.0)	1/3 (2.5 ± 1.44)	1/3 (1.0 ± 0.0)	1/3 (1.5 ± 0.0)	0/3 (0.0 ± 0.0)	1/3 (2.0 ± 0.0)	1/3 (1.0 ± 0.0)
690OP	3	2/3 (3.0 ± 0.7)	2/3 (2.00 ± 1.41)	2/3 (2.0 ± 0.7)	1/3 (2.0 ± 0.0)	0/3 (0.0 ± 0.0)	2/3 (3.50 ± 0.0)	1/3 (1.5 ± 0.0)
	7	0/3 (0.0 ± 0.0)	0/3 (0.00 ± 0.0)	1/3 (1.0 ± 0.0)	0/3 (0.0 ± 0.0)	0/3 (0.0 ± 0.0)	0/3 (0.0 ± 0.0)	0/3 (0.0 ± 0.0)

[1]$\log_{10}$ EID_{50}/ml

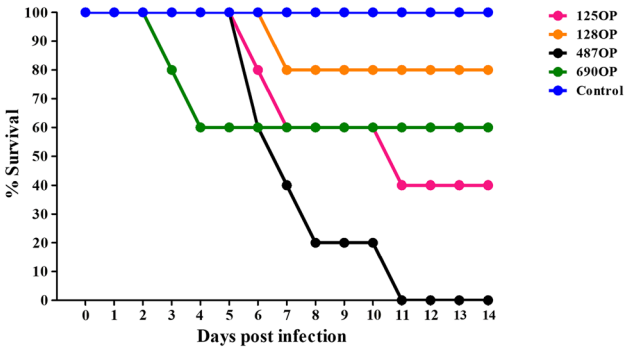

Fig. 3 A plot of the Kaplan–Meier estimator survival rate of C57BL/6 mice infected with the four H7N3 strains. To analyze differences in the replication of these four H7N3 viruses, eight mice were used for each group. Three mice were euthanized at 3 dpi, and five mice remained under observation, with mortality and loss of body weight recorded for 14 days. H7N3 487OP was the most pathogenic in mice, with no survival after 11 days.

Replication of H7N3 viruses in C57BL/6 mice

Shedding was observed in each of the four groups of mice infected with one of the four different H7N3 viruses. The virus 487OP was lethal in all of the infected mice by 10 dpi (100% mortality), while the viruses 125OP, 128OP, and 690OP caused 60, 20, and 40% mortality, respectively (Fig. 3). Mice infected with 125OP showed early infection at 3 dpi and remained infected until 7 dpi, with the highest level of viral shedding at 7 dpi (1.75 $\log_{10}$ EID_{50}/ml), while infection with 128OP continued for 3 dpi (1.5 $\log_{10}$ EID_{50}/ml). Infection with 487OP continued until 7 dpi and the virus was shed at high titers at 3 dpi (1.83 $\log_{10}$ EID_{50}/ml), while infection with 690OP continued until 5 dpi, with the highest viral shedding at 3 dpi (1.83 $\log_{10}$ EID_{50}/ml) (Table 4).

Table 4 Replication and transmission of H7N3 viruses in C57BL/6 mice

Group	Sample	Number of infected/inoculated mice (mean virus titer[1] ± SD)		
		Days postinfection		
		3	5	7
Inoculated 125OP	Nasal wash	1/3 (1.5 ± 0.00)	2/3 (1.5 ± 0.70)	2/3 (1.75 ± 0.35)
Inoculated 128OP	Nasal wash	2/3 (1.5 ± 0.00)	0/3 (0.00 ± 0.00)	0/3 (0.00 ± 0.00)
Inoculated 487OP	Nasal wash	3/3 (1.83 ± 0.57)	3/3 (1.16 ± 0.28)	1/2 (1.50 ± 0.00)
Inoculated 690OP	Nasal wash	1/3 (2.0 ± 0.00)	1/3 (1.5 ± 0.86)	0/3 (0.00 ± 0.00)

[1]$\log_{10}$ EID_{50}/ml

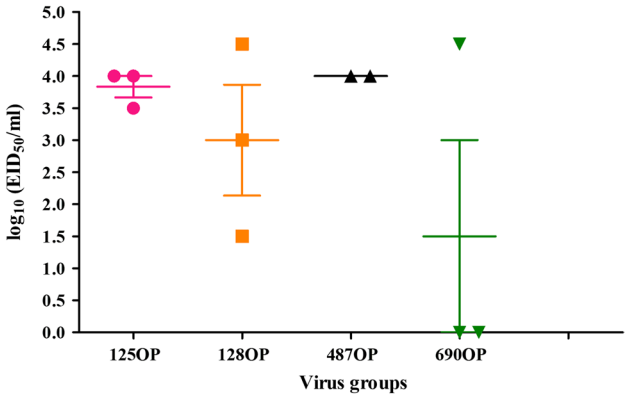

Fig. 4 Virus shedding in lung tissue of mice three days after infection with the four H7N3 strains. Virus propagation in lung tissue was titrated by EID_{50}, with three mice from each infected group. A mouse was found dead in the 487OP group.

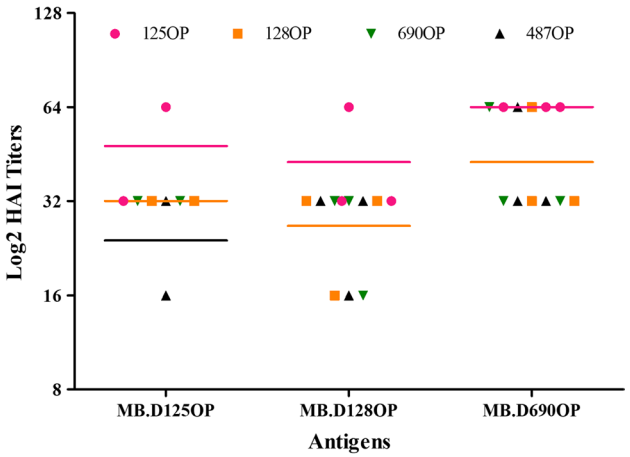

Fig. 5 Antibody titers expressed as log_2, showing that 125OP and 128OP induced antibodies against all of the viruses, with the highest titer against 125OP. 690OP induced similar levels of antibodies against all four viruses.

All of the H7 viruses replicated efficiently in the lungs of mice (Fig. 4). All three mice infected with 125OP were positive, and the mean EID_{50} titer was 3.8 log_{10} EID_{50}/ml, while the mean was 3 log_{10} EID_{50}/ml for 128OP and 1.5 log_{10} EID_{50}/ml for 690OP. The titer of 487OP was the highest of all of the viruses; the mean EID_{50} was 4 log_{10} EID_{50}/ml.

Cross-reactivity of collected sera detected by HI assay

All of the sera collected from infected mice showed cross-reactivity with each other (Fig. 5). In addition, the sera collected from mice infected with 125OP showed a high antibody titer against all of the viruses, up to 64 log_2.

Histopathological examination

Lung

Histopathological examination of the lungs of 125OP-virus-infected chickens revealed severe interstitial pneumonia, degenerated bronchi, and a large amount of cellular debris filling the lung alveoli. The lungs infected with 128OP exhibited pneumonia and a ruptured arteriolar wall with thrombus formation. The lungs of the 487OP-virus-infected chickens showed collapsed alveoli and extensive hemorrhagic bronchopneumonia with massive infiltration of the lung parenchyma with inflammatory cells and RBCs. Chickens infected with 690OP showed inflammatory cell infiltration in the lungs and compensatory bronchiectasis with disruption of the bronchiolar wall (Fig. 6a-e).

Trachea

Histological evaluation of the trachea of 125OP-virus-infected chickens showed dense inflammatory cellular infiltration with lymphocytes, macrophages, and neutrophils invading the mucosal and submucosal layers and the lamina propria, whereas the trachea of the 128OP-virus-infected chickens showed exfoliation and sloughing of the tracheal epithelium along with edema of the lamina propria. The trachea of the 487OP-virus-infected chickens displayed marked activation of the mucus-secreting glands with goblet cell hypertrophy in addition to tracheal epithelial degeneration and diffuse lymphocytic infiltration. The 690OP-virus-infected chickens showed a denuded tracheal epithelium and complete loss of cilia (Fig. 6f-j).

Intestine

Examination of the intestines of 125OP-virus-infected chickens revealed a loss of the regular architecture of the villi, with degeneration and disruption of the villous epithelium. 128OP, on the other hand, caused intestinal villous necrobiosis with shedding of the necrotic epithelium into the intestinal lumen. The intestines of 487OP-virus-infected chickens showed dense lymphocytic infiltration with broadening and fusion of the intestinal villi, while 690OP-virus-infected intestines displayed detachment of the villi, villous disfigurement, and increased numbers of goblet cells (Fig. 6k-o).

Liver

Examination of the livers of 125OP-virus-infected chickens showed disrupted hepatic architecture with marked shrinkage and irregularity of the hepatocyte cords along with obvious dilatation of the hepatic sinusoids. 128OP-virus-infected chickens displayed congestion of the central vein

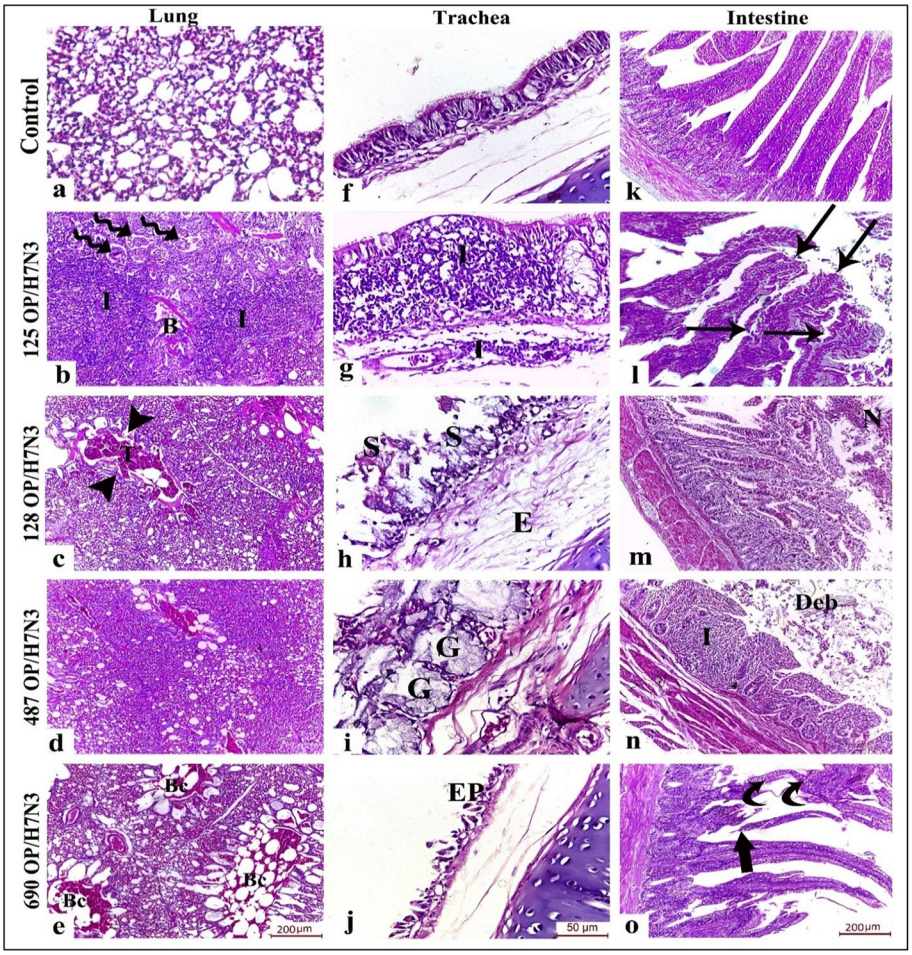

Fig. 6 Histological analysis of lungs, trachea, and intestines of birds exposed to different viruses compared to healthy uninfected controls. (a-e) H&E-stained sections of lungs. (a) Control group showing normal lung architecture with patent alveoli. (b) Infection with virus 125OP, showing severe interstitial pneumonia in lung tissues, where the alveoli appear to be flooded with inflammatory cells (I). Note degenerated bronchi (B) and numerous alveoli filled with desquamated cells and cellular debris (spiral arrows). (c) Infection with virus 128OP, showing pneumonia and a ruptured arteriolar wall (arrow heads) with thrombus formation (T). (d) Infection with virus 487OP, showing extensive hemorrhagic bronchopneumonia with massive infiltration of the lung parenchyma with inflammatory cells and RBCs and collapsed alveoli. (e) Infection with virus 690OP, showing inflammatory infiltration and compensatory bronchiectasis (Bc) with destruction of the bronchiolar wall. (f-j) Trachea. (f) Control group showing normal histological structure of the trachea with intact pseudostratified columnar ciliated epithelium and lamina propria. (g) Infection with virus 125OP, showing dense inflammatory cellular infiltration (I) invading the mucosal and submucosal layers and the lamina propria. (h) Infection with virus 128OP, showing exfoliation and sloughing (S) of the tracheal epithelium along with edema (E) of the lamina propria. (i) Infection with virus 487OP, showing marked activation of the mucous secreting glands (G) with goblet cell hypertrophy and degeneration of the tracheal epithelial cells with diffuse lymphocytic infiltration. (j) Infection with virus 690OP, showing denuded tracheal epithelium (EP) with a complete loss of cilia. (k-o) Intestine (k) Control group showing normal finger-like intestinal villi with a core of connective tissue, healthy epithelial covering, and a few goblet cells. (l) Infection with virus 125OP, showing loss of the regular architecture of the villi with degeneration and disruption of the villous epithelium (arrows). (m) Infection with virus 128OP, showing intestinal villous necrobiosis with shedding of the necrotic epithelium (N) into the intestinal lumen. (n) Infection with virus 487OP, showing dense lymphocytic infiltration (I) with broadening and fusion of the intestinal villi. Note the presence of desquamated cellular debris (Deb) in the intestinal lumen. (o) Infection with virus 690OP, showing detachment of the villi (thick arrow), villous disfigurement, and increased goblet cells (curved arrows)

and localized areas of inflammation. 487OP-virus-infected chickens displayed massive areas of hepatic necrosis invaded by inflammatory infiltration, while 690OP-virus-infected chickens showed marked dilatation and congestion of the central vein with multiple foci of cellular necrosis and bridging fibrosis (Fig.7a-e).

Bursa of Fabricius

The bursae of Fabricius of the 125OP-virus-infected chickens showed irregularity of the basement membrane between the cortex and medulla of the lymphoid follicles together with vascular congestion and proliferation of intra-follicular

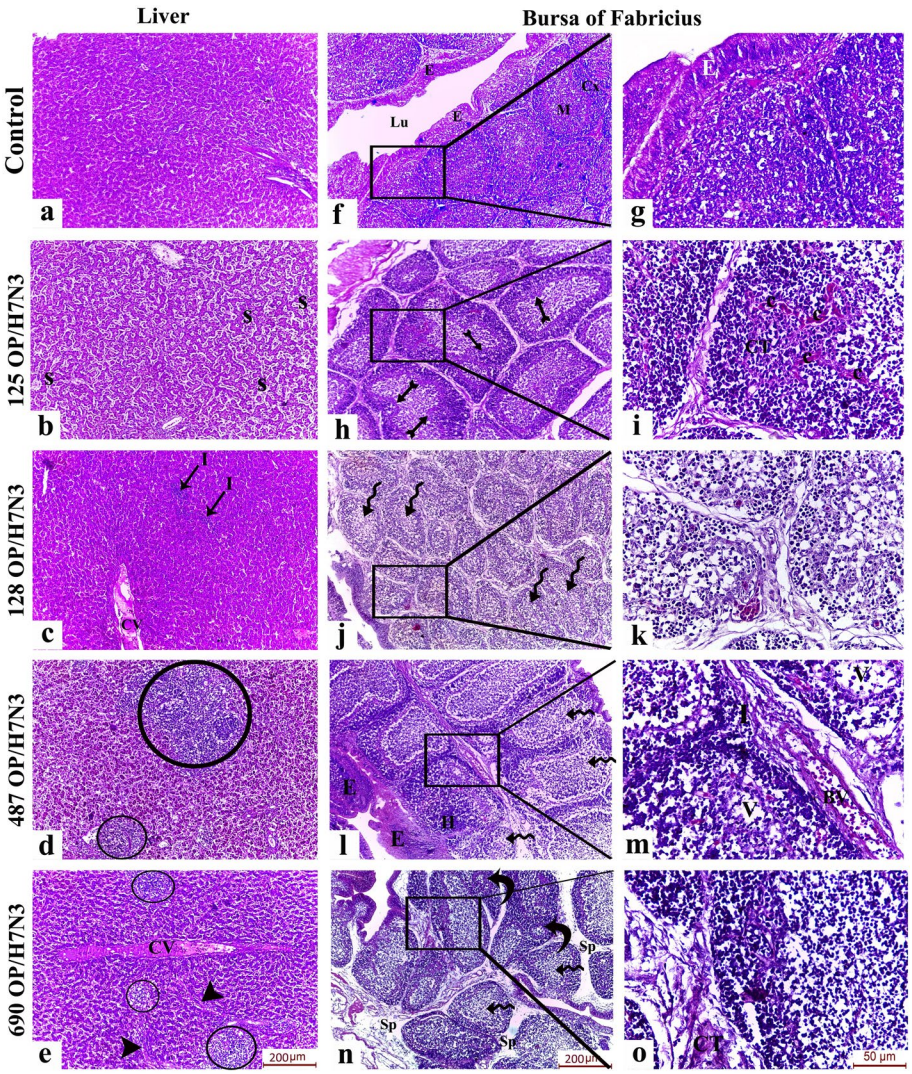

Fig. 7 (a-e) H&E-stained sections of liver. (a) Control group showing regular plates of hepatocytes radiating from the central vein towards the portal area. (b) Virus 125OP, showing disrupted hepatic architecture with marked shrinkage and irregularity of the hepatocyte cords along with obvious dilatation of the hepatic sinusoids (S). (c) Virus 128OP, showing congestion of the central vein (CV) and localized areas of inflammation (I). (d) Virus 487OP, showing massive areas of hepatic necrosis invaded by inflammatory infiltration (circles). (e) Virus 690OP, showing marked dilatation and congestion of the central vein (CV) with multiple foci of cellular necrosis (circles) and bridging fibrosis (arrowheads). (f-o) Bursa of Fabricius. (f) Control group showing normal histological structure of the bursa with crypt-like folds lined by epithelium (E) surrounding the lumen (Lu) and enclosing tightly-packed lymphoid follicles formed of cortex (Cx) and medulla (M) with thin inter-follicular tissue. (g) Higher magnification of the control group showing large, densely populated bursal follicles enclosed by stratified squamous epithelium (E). (h) Virus 125OP, showing irregularity of the basement membrane between the cortex and medulla of the lymphoid follicles (tailed arrows). (i) Higher magnification of virus 125OP, showing vascular congestion (c) and proliferation of intra-follicular connective tissue (CT). (j) Virus 128OP, showing severe lymphoid depletion and necrosis of the follicles (spiral arrows). (k) Higher magnification of virus 128OP, showing marked depletion of lymphocytes in the bursal follicle, leaving numerous empty spaces. (l) Virus 487OP, showing marked epithelial thickening (E), some areas of lymphocyte hyperplastic changes (H), and others with lymphocyte depletion (spiral arrows). (m) Higher magnification of virus 487OP, showing vacuolation (V) of the lymphoid follicles, a dilated inter-follicular blood vessel (BV), and infiltration of the inter-follicular tissue with mononuclear cells. (n) Virus 690 OP showing disruption and atrophy of the follicles with widening of the inter-follicular spaces (Sp), lymphocyte depletion (spiral arrows), and cyst formation (curved arrows). (o) Higher magnification of virus 690OP, showing proliferation of the inter-follicular stromal connective tissue and infiltration with mononuclear cells.

connective tissue. Infection with 128OP caused severe lymphoid depletion and necrosis of the follicles. 487OP-virus-infected chickens showed marked epithelial thickening, some areas of lymphocyte hyperplasia, other areas with lymphocyte depletion, and dilated inter-follicular blood vessels. The bursae of chickens infected with 690OP showed

disruption and atrophy of the follicles with widening of the inter-follicular spaces, lymphocyte depletion, cyst formation, and proliferation of the inter-follicular stromal connective tissue with infiltration of mononuclear cells (Fig. 7f-o).

Antiviral properties of FDA-approved antiviral drugs against H7N3

The cytotoxicity of the antiviral drugs oseltamivir, zanamivir, amantadine, favipiravir, and remdesivir (Fig. 8) in MDCK cells was determined by MTT assay. The safest compound was favipiravir, with the highest CC_{50} of 1249 µM, followed by zanamivir. Oseltamivir had the lowest CC_{50} of 516.3 µM (Table 5).

The antiviral potential of commercial antiviral drugs against the four H7N3 strains was tested and compared to their antiviral activity against strain A/Puerto Rico/8/34 (H1N1) (Fig. 9). The strongest antiviral activity against the viruses tested in the current study was observed with favipiravir, with an IC_{50} of 3.9, 6.02, 5.4, 4.5, and 57.7 µM against 125OP, 128OP, 487OP, 690OP, and H1N1, respectively. The lowest antiviral activity was observed with remdesivir, which exhibited low antiviral activity with all of the viruses tested. On the other hand, zanamivir had a notable effect on 125OP and 487, with an IC_{50} of 17.09 and 14.05 µM, respectively. Oseltamivir had an antiviral effect against 690OP and 487OP, with an IC_{50} of 6.456 and 15.68 µM, respectively. Amantadine was able

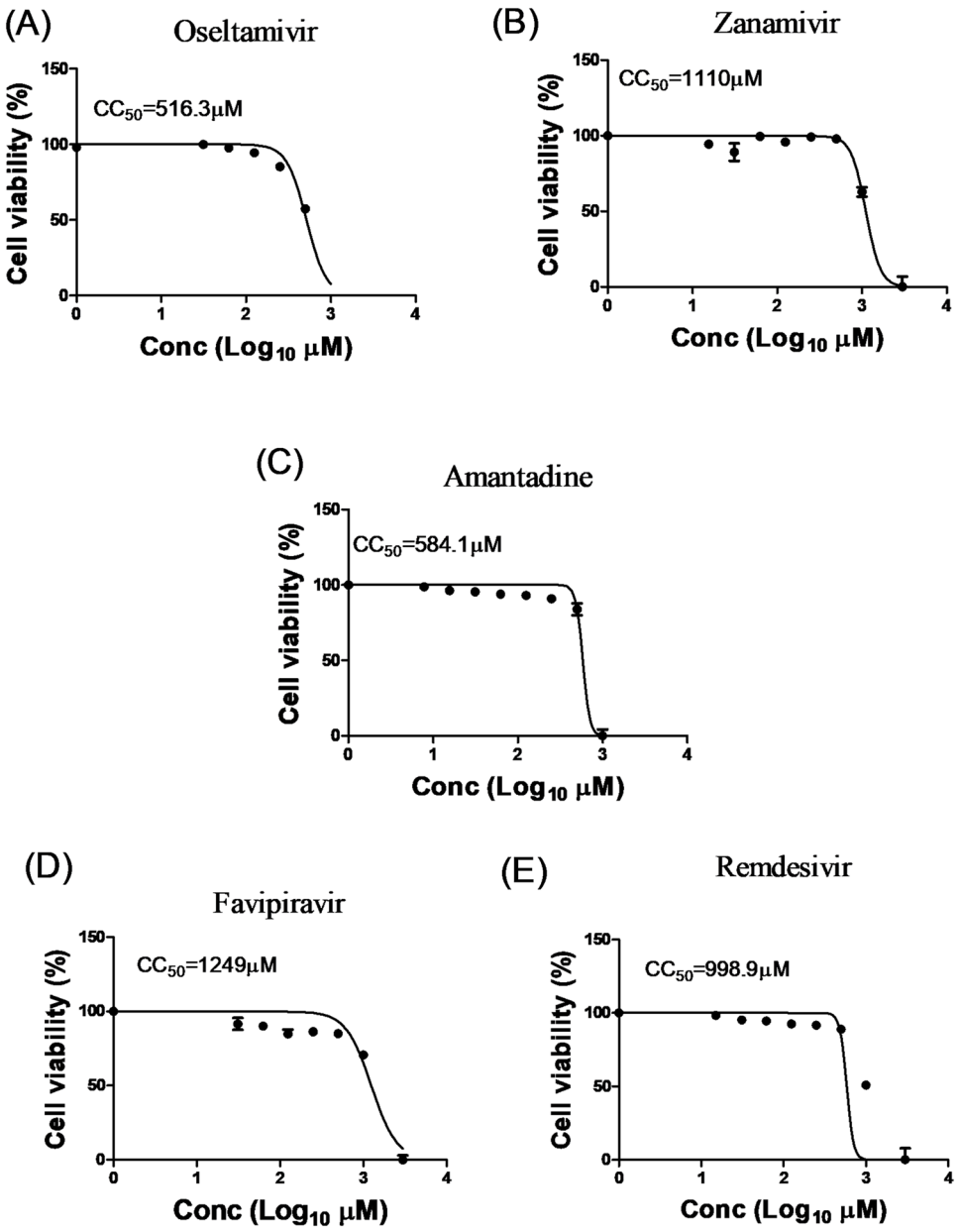

Fig. 8 Cytotoxicity of the FDA-approved antiviral drugs oseltamivir, zanamivir, amantadine, favipiravir, and remdesivir in MDCK cells. The viability of MDCK cells was measured at various concentrations of (A) oseltamivir, (B) zanamivir, (C) amantadine, (D) favipiravir, and (E) remdesivir, and the 50% cytotoxicity concentration (CC_{50}) of each drug was calculated using nonlinear regression analysis in Graph Pad Prism software.

Table 5 CC_{50}, IC_{50}, and SI per micromole of the FDA-approved antiviral drugs oseltamivir, zanamivir, amantadine, favipiravir, and remdesivir against the four H7N3 strains and A/Puerto Rico/8/34 (H1N1)

Drug	CC_{50}	IC_{50} 125OP	IC_{50} 128OP	IC_{50} 487OP	IC_{50} 690OP	IC_{50} H1N1	SI 125OP	SI 128OP	SI 487OP	SI 690OP	SI H1N1
Favipiravir	1249	3.9	6.024	5.4	4.5	57.7	320.2	207.3	231.3	277.5	21.6
Zanamivir	1110	17.09	84.97	14.05	23.3	180	64.95	13.06	79	47.6	6.16
Oseltamivir	516.3	407.7	85.7	15.68	6.456	51.16	1.2	6.02	33.1	78.9	10.1
Amantadine	584.1	17.02	45.17	5.17	6.5	77.3	34.3	12.9	112.8	88.8	7.5
Remdesivir	996.9	44.5	25.97	19.1	41.6	140.3	22.3	38.3	52.16	23.9	7.1

CC_{50}, half-maximal cytotoxic concentration; IC_{50}, half-maximal inhibitory concentration; SI, safety index (CC_{50}/IC_{50})

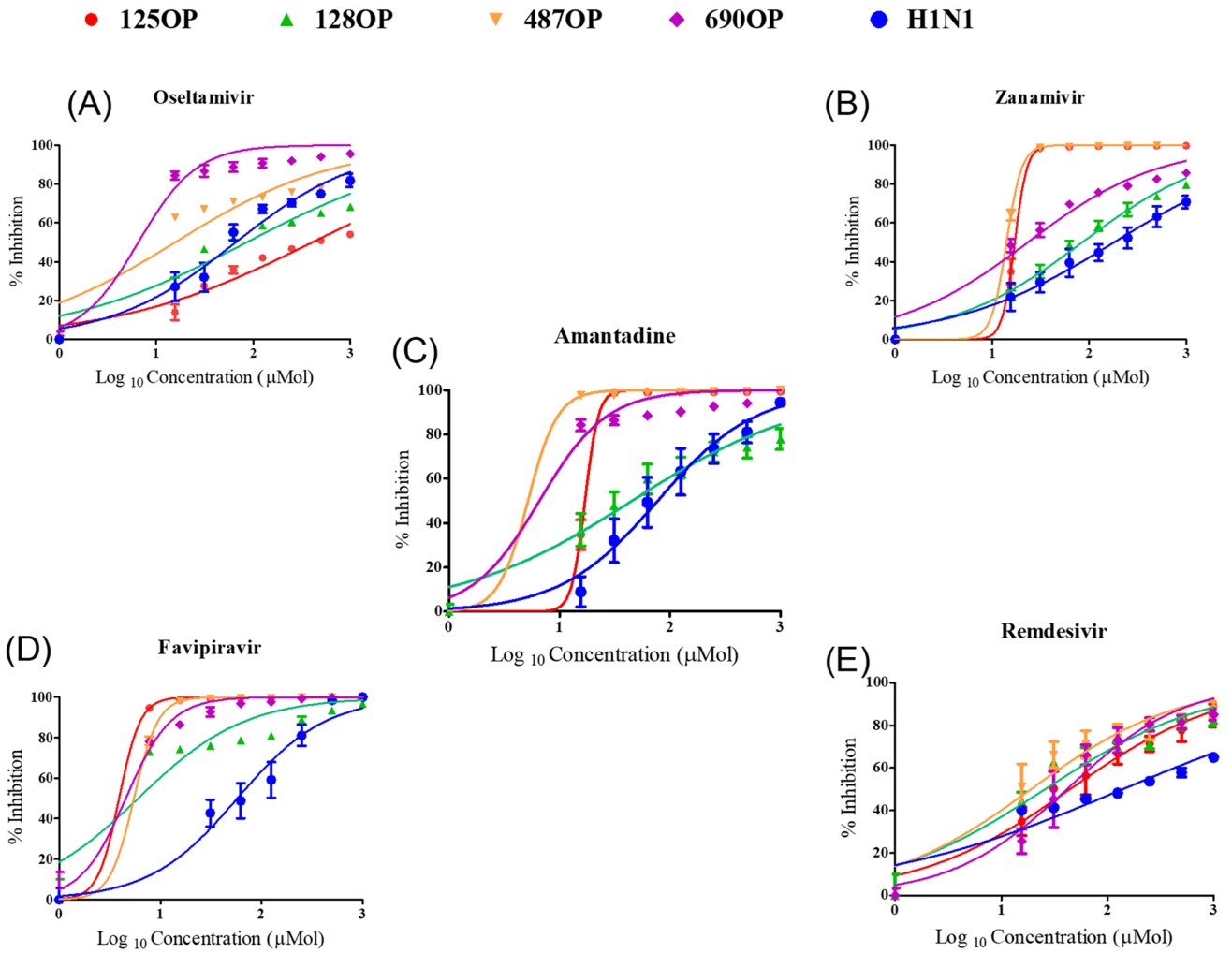

Fig. 9 Antiviral activity of the FDA-approved antiviral drugs oseltamivir, zanamivir, amantadine, favipiravir, and remdesivir against the four H7N3 strains and A/Puerto Rico/8/34 (H1N1). The antiviral activity of (A) oseltamivir, (B) zanamivir, (C) amantadine, (D) favipiravir, and (E) remdesivir was tested. The 50% inhibitory concentration (IC_{50}) of each tested drug was calculated using nonlinear regression analysis in triplicate for each concentration used. The best-fitting line was drawn between log concentrations and percent viral inhibition using Graph Pad Prism software.

to inhibit 487OP and 690OP, with an IC_{50} of 5.17 and 6.5 µM, respectively. The safety index (SI) was calculated to determine the safest antiviral drug against the four H7N3

viruses tested in this study. Our results showed that favipiravir was the safest of these drugs.

We studied the antiviral resistance of the four H7N3 isolates by analysis of their genomes in comparison to strain A/Puerto Rico/8/34 (H1N1) to determine if site mutations known to cause a decrease in susceptibility to antiviral agents were present. All viruses tested in this study displayed resistance to M2 blocker despite not having a known mutation associated with remdesivir resistance (Table 6). Also, none of the common mutations associated with resistance to neuraminidase inhibitors were present (Table 7).

Discussion

Understanding the antigenic diversity of H7 AIVs is critical for developing effective strategies for disease prevention and control [9]. In previous studies, we observed different genetic constellations within four H7N3 viruses isolated in the same migration season (Fig. 1). All of the isolates belonged to the Eurasian lineage. Genetic analysis of these viruses showed that all of them were LPAIVs, and their HA cleavage sites had the motif 333PELPKGRGLF342, which enables the viruses to circulate for a considerable time in domestic poultry with the potential of acquiring HPAIV characteristics. Wild birds are able to carry viruses over long distances, and infection spillover into domestic poultry can cause the virus to change from an LPAIV to an HPAIV [20]. Infection of the same host with multiple viruses increases the chance of genetic reassortment and the emergence of new influenza virus strains with pandemic potential, as has been the case in pandemics involving viruses with an HA gene of avian origin [34, 43].

The majority of previous studies examining the pathogenicity of influenza viruses in different avian hosts have shown lower susceptibility of chickens than other avian hosts [37, 40]. HPAIV infection causes systemic symptoms leading to high mortality in gallinaceous species [29], while LPAIVs cause mild or asymptomatic infections with a disturbance in egg production [30]. In the current study, the LPAIV H7 strains in chickens were shed longer by the cloacal route than by the oropharyngeal route, with the virus still detectable at 10 dpi. Ocular edema was the only clinical sign observed in all chicken groups infected with the four H7N3 viruses. Wild ducks infected with LPAIV H7 subtypes usually shed the virus through feces [8]. The viruses were detected in systemic tissues of inoculated chickens, which could suggest that they had acquired genetic changes that enabled dissemination by mechanisms typical of HPAIV infection. The postmortem examination of collected organs showed severe systemic pathological signs in inoculated chickens, which indicates that these viruses are highly virulent in chickens.

Table 6 Genotypic markers and site mutations associated with resistance to M2 blockers

Virus type	Phenotype					Susceptibility (S) Resistance (R)
	26I	27A	31N	33A	34E	
125OP/2015 (H7N3)	L	V	S	I	G	S
128OP/2015 (H7N3)	L	V	S	I	G	S
487OP/2016 (H7N3)	L	V	S	I	G	S
690OP/2016 (H7N3)	L	V	S	I	G	S
A/Puerto Rico /8/34(H1N1)	L	V	N	I	G	R

Table 7 Genotypic markers and site mutations associated with resistance to neuraminidase inhibitors

Virus type	Phenotype									Susceptibility (S) Resistance (R)
	Y155H	E258Q	D198G	H274Y	Q136K	E119G	N294S	V116A	I222L	
125OP (H7N3)	Y	E	D	H	Q	E	N	V	I	S
128OP (H7N3)	Y	E	D	H	Q	E	N	V	I	S
487OP (H7N3)	Y	E	D	H	Q	E	N	V	I	S
690OP (H7N3)	Y	E	D	H	Q	E	N	V	I	S
A/Puerto Rico /8/34 (H1N1)	Y	E	D	H	Q	E	N	V	I	S

Human infections with H7 viruses have been reported with increased frequency since 2002 [4], and two cases of human infection with LPAIV H7N3 reported in Canada in 2004 were attributed to direct contact with infected poultry [36]. In Norfolk, UK, an outbreak of LPAIV H7N3 was reported in 2006, associated with human infection diagnosed as conjunctivitis [26]. We compared the relative virulence of H7 virus isolates in a mammalian host. All viruses replicated well in C57BL/6 mice and were shed for a duration of more than 7 dpi without previous adaptation to the mammalian host, which is a significant indicator of potential human infection. One of the four strains, 487OP, was more virulent than the others and killed all of the infected mice (Fig. 3). The viruses replicated efficiently in the lungs, and this could be correlated with mortality. The ability of LPAIVs to replicate robustly in a mammalian host with fatal results indicates that these studies should be extended to other mammalian models.

The mammalian replication results led us to examine the sensitivity of those viruses to commercial antivirals. Each strain showed a different pattern of resistance to different antiviral families. 125OP showed the most resistance to neuraminidase inhibitors, while 128OP virus showed the most resistance to M2 blocker antivirals. RNA inhibitors appear to be a good choice since all four strains showed sensitivity toward them, and they can be used against a wide range of viruses [35]. In a previous study to determine the sensitivity of H7 viruses to neuraminidase inhibitors *in vivo*, mice were infected by the ocular route with A/Canada/504/2004 virus (H7N3 [Can/504]), and the results showed that the infection did not cause substantial morbidity, although efficient replication was detected in ocular tissue [5].

H7 viruses should not be underestimated. Many research articles have compared the pathogenicity of H5 and H7 viruses, but what is interesting is the abundance of H7 isolates in migratory birds, whereas H5 viruses have been endemic in Egypt since 2006. Hence, it is important to continue monitoring H7 and other subtypes as they circulate in their natural reservoirs, migratory waterfowl.

Acknowledgments The authors acknowledge Human Link DMCC as a grant supporter. The authors would like to thank Mrs. Rebecca Badra for editing the manuscript.

Author contributions Conceptualization, NFA, GK, MAA, MAR; methodology, AK, GK, MAA; formal analysis, AEK, OK, AK; investigation, AEK, OK, YM, AET, BEA; data curation, AEK, OK, YM, AET, BEA; writing – original draft preparation, AEK, OK, AK, YM; writing –review and editing, NFA, GK, MAA, MAR; supervision, NFA, GK, MAA, MAR; funding acquisition, GK, MAA. All authors have read and agreed to the published version of the manuscript.

Funding This research was funded by the National Institute of Allergy and Infectious Diseases, National Institutes of Health, and US Department of Health and Human Services (under contract numbers HHSN272201400006C and 75N93021C00016).

Data availability statement All data are available within the manuscript.

Declarations

Conflict of interest The authors have no relevant financial or non-financial interests to disclose.

Ethical approval This study was performed in line with the principles of the Declaration of Helsinki. Animal experiments were approved by the Medical Research Ethics Committee of the National Research Centre (ethical permission code: 18040, April 2018).

References

1. Abbas MA, Spackman E, Swayne DE, Ahmed Z, Sarmento L, Siddique N, Naeem K, Hameed A, Rehmani S (2010) Sequence and phylogenetic analysis of H7N3 avian influenza viruses isolated from poultry in Pakistan 1995–2004. Virol J 7:137
2. Alexander DJ (2000) A review of avian influenza in different bird species. Vet Microbiol 74:3–13
3. Banks J, Speidel ES, Moore E, Plowright L, Piccirillo A, Capua I, Cordioli P, Fioretti A, Alexander DJ (2001) Changes in the haemagglutinin and the neuraminidase genes prior to the emergence of highly pathogenic H7N1 avian influenza viruses in Italy. Arch Virol 146:963–973
4. Belser JA, Bridges CB, Katz JM, Tumpey TM (2009) Past, present, and possible future human infection with influenza virus A subtype H7. Emerg Infect Dis 15:859–865
5. Belser JA, Sleeman K, Pearce MB, Katz JM, Gubareva LV, Tumpey TM (2012) Oseltamivir inhibits H7 influenza virus replication in mice inoculated by the ocular route. Antimicrob Agents Chemother 56:1616–1618
6. Berhane Y, Hisanaga T, Kehler H, Neufeld J, Manning L, Argue C, Handel K, Hooper-McGrevy K, Jonas M, Robinson J, Webster RG, Pasick J (2009) Highly pathogenic avian influenza virus A (H7N3) in domestic poultry, Saskatchewan, Canada, 2007. Emerg Infect Dis 15:1492–1495
7. Bernas T, Dobrucki J (2002) Mitochondrial and nonmitochondrial reduction of MTT: Interaction of MTT with TMRE, JC-1, and NAO mitochondrial fluorescent probes. Cytometry 47:236–242
8. Costa TP, Brown JD, Howerth EW, Stallknecht DE (2011) Variation in viral shedding patterns between different wild bird species infected experimentally with low-pathogenicity avian influenza viruses that originated from wild birds. Avian Pathol 40:119–124
9. Criado MF, Leyson CM, Youk S, DeBlois S, Olivier T, Killian ML, Torchetti ML, Parris DJ, Spackman E, Kapczynski DR, Suarez DL, Swayne DE, Pantin-Jackwood MJ (2021) The pathobiology of H7N3 low and high pathogenicity avian influenza viruses from the United States outbreak in 2020 differs between Turkeys and Chickens. Viruses 13(9):1851. https://doi.org/10.3390/v13091851. PMID: 34578433; PMCID: PMC8472980
10. Diaz A, Marthaler D, Corzo C, Muñoz-Zanzi C, Sreevatsan S, Culhane M, Torremorell M (2017) Multiple genome constellations of similar and distinct influenza A viruses co-circulate in pigs during epidemic events. Sci Rep 7:11886
11. Diskin ER, Friedman K, Krauss S, Nolting JM, Poulson RL, Slemons RD, Stallknecht DE, Webster RG, Bowman AS (2020) Subtype diversity of influenza A virus in North American Waterfowl: a Multidecade Study. J Virol 94(11):e02022–19. https://doi.org/10.1128/JVI.02022-19. PMID: 32188732; PMCID: PMC7269424

12. Gaush CR, Smith TF (1968) Replication and plaque assay of influenza virus in an established line of canine kidney cells. Appl Microbiol 16:588–594
13. Goldhill DH, Velthuis AJWT, Fletcher RA, Langat P, Zambon M, Lackenby A, Barclay WS (2018) The mechanism of resistance to favipiravir in influenza. Proc Natl Acad Sci 115:11613–11618
14. Hirst M, Astell CR, Griffith M, Coughlin SM, Moksa M, Zeng T, Smailus DE, Holt RA, Jones S, Marra MA, Petric M, Krajden M, Lawrence D, Mak A, Chow R, Skowronski DM, Tweed SA, Goh S, Brunham RC, Robinson J, Bowes V, Sojonky K, Byrne SK, Li Y, Kobasa D, Booth T, Paetzel M (2004) Novel avian influenza H7N3 strain outbreak, British Columbia. Emerg Infect Dis 10:2192–2195
15. Huprikar J, Rabinowitz S (1980) A simplified plaque assay for influenza viruses in Madin-Darby kidney (MDCK) cells. J Virol Methods 1:117–120
16. Kayed AS, Kandeil A, Gomaa MR, El-Shesheny R, Mahmoud S, Hegazi N, Fayez M, Sheta B, McKenzie PP, Webby RJ, Kayali G, Ali MA (2019) Surveillance for avian influenza viruses in wild birds at live bird markets, Egypt, 2014–2016. Influenza Other Respir Viruses 13:407–414
17. Kim HR, Kwon YK, Jang I, Lee YJ, Kang HM, Lee EK, Song BM, Lee HS, Joo YS, Lee KH, Lee HK, Baek KH, Bae YC (2015) Pathologic changes in wild birds infected with highly pathogenic avian influenza A(H5N8) viruses, South Korea, 2014. Emerg Infect Dis 21:775–780
18. Krammer F, Smith GJD, Fouchier RAM, Peiris M, Kedzierska K, Doherty PC, Palese P, Shaw ML, Treanor J, Webster RG, Garcia-Sastre A (2018) Influenza. Nat Rev Dis Primers 4:3
19. Krauss S, Webster RG (2010) Avian influenza virus surveillance and wild birds: past and present. Avian Dis 54:394–398
20. Lee DH, Criado MF, Swayne DE (2021) Pathobiological origins and evolutionary history of highly pathogenic avian influenza viruses. Cold Spring Harb Perspect Med 11(2):a038679. https://doi.org/10.1101/cshperspect.a038679. PMID: 31964650; PMCID: PMC7849344
21. Lee YN, Lee DH, Cheon SH, Park YR, Baek YG, Si YJ, Kye SJ, Lee EK, Heo GB, Bae YC, Lee MH, Lee YJ (2020) Genetic characteristics and pathogenesis of H5 low pathogenic avian influenza viruses from wild birds and domestic ducks in South Korea. Sci Rep 10:12151
22. McKimm-Breschkin JL (2013) Influenza neuraminidase inhibitors: antiviral action and mechanisms of resistance. Influenza Other Respir Viruses 7:25–36
23. Moatasim Y, Kandeil A, Aboulhoda BE, El-Shesheny R, Alkhazindar M, AbdElSalam ET, Kutkat O, Kamel MN, El Taweel AN, Mostafa A, Hicks JT, Abd Elghaffar SK, Kayali G, Ali MA (2019) Comparative virological and pathogenic characteristics of avian influenza H5N8 viruses detected in wild birds and domestic poultry in Egypt during the winter of 2016/2017. Viruses 11(11):990. https://doi.org/10.3390/v11110990. PMID: 31717865; PMCID: PMC6893538
24. Mostafa A, Kandeil A, Elshaier AMMY, Kutkat O, Moatasim Y, Rashad AA, Shehata M, Gomaa MR, Mahrous N, Mahmoud SH, GabAllah M, Abbas H, Taweel AE, Kayed AE, Kamel MN, Sayes ME, Mahmoud DB, El-Shesheny R, Kayali G, Ali MA (2020) FDA-approved drugs with potent in vitro antiviral activity against severe acute respiratory syndrome coronavirus 2. Pharmaceuticals 13:443
25. Neumann G, Noda T, Kawaoka Y (2009) Emergence and pandemic potential of swine-origin H1N1 influenza virus. Nature 459:931–939
26. Nguyen-Van-Tam JS, Nair P, Acheson P, Baker A, Barker M, Bracebridge S, Croft J, Ellis J, Gelletlie R, Gent N, Ibbotson S, Joseph C, Mahgoub H, Monk P, Reghitt TW, Sundkvist T, Sellwood C, Simpson J, Smith J, Watson JM, Zambon M, Lightfoot N, Incident Response T (2006) Outbreak of low pathogenicity H7N3 avian influenza in UK, including associated case of human conjunctivitis. Euro Surveill 11(E060504):060502
27. OFFLU (2022) OFFLU AVIAN INFLUENZA VCM REPORT September 2021 to February 2022. In this document we present a summary of H5, H7 and H9 avian influenza A virus events reported from 1st September 2021 to 1st February 2022. OFFLU WHO VCM datapackage, OFFLU WHO VCM datapackage
28. Olsen B, Munster VJ, Wallensten A, Waldenstrom J, Osterhaus AD, Fouchier RA (2006) Global patterns of influenza a virus in wild birds. Science 312:384–388
29. Pantin-Jackwood MJ, Swayne DE (2009) Pathogenesis and pathobiology of avian influenza virus infection in birds. Rev Sci Tech 28:113–136
30. Peng Y, Xie ZX, Liu JB, Pang YS, Deng XW, Xie ZQ, Xie LJ, Fan Q, Luo SS (2013) Epidemiological surveillance of low pathogenic avian influenza virus (LPAIV) from poultry in Guangxi Province, Southern China. PLoS ONE 8:e77132
31. Reed LJ, Muench H (1938) A simple method of estimating fifty per cent endpoints12. Am J Epidemiol 27:493–497
32. Rohm C, Horimoto T, Kawaoka Y, Suss J, Webster RG (1995) Do hemagglutinin genes of highly pathogenic avian influenza viruses constitute unique phylogenetic lineages? Virology 209:664–670
33. Rojas H, Moreira R, Avalos P, Capua I, Marangon S (2002) Avian influenza in poultry in Chile. Vet Rec 151:188
34. Schafer JR, Kawaoka Y, Bean WJ, Suss J, Senne D, Webster RG (1993) Origin of the pandemic 1957 H2 influenza A virus and the persistence of its possible progenitors in the avian reservoir. Virology 194:781–788
35. Shiraki K, Daikoku T (2020) Favipiravir, an anti-influenza drug against life-threatening RNA virus infections. Pharmacol Ther 209:107512
36. Skowronski DM, Tweed SA, Petric M, Booth T, Li Y, Tam T (2006) Human illness and isolation of low-pathogenicity avian influenza virus of the H7N3 subtype in British Columbia, Canada. J Infect Dis 193:899–900 (**author reply 900-891**)
37. Spackman E, Gelb J Jr, Preskenis LA, Ladman BS, Pope CR, Pantin-Jackwood MJ, McKinley ET (2010) The pathogenesis of low pathogenicity H7 avian influenza viruses in chickens, ducks and turkeys. Virol J 7:331
38. Stallknecht DE, Shane SM (1988) Host range of avian influenza virus in free-living birds. Vet Res Commun 12:125–141
39. Suarez DL, Senne DA, Banks J, Brown IH, Essen SC, Lee CW, Manvell RJ, Mathieu-Benson C, Moreno V, Pedersen JC, Panigrahy B, Rojas H, Spackman E, Alexander DJ (2004) Recombination resulting in virulence shift in avian influenza outbreak, Chile. Emerg Infect Dis 10:693–699
40. Tumpey TM, Kapczynski DR, Swayne DE (2004) Comparative susceptibility of chickens and turkeys to avian influenza A H7N2 virus infection and protective efficacy of a commercial avian influenza H7N2 virus vaccine. Avian Dis 48:167–176
41. Wang C, Takeuchi K, Pinto LH, Lamb RA (1993) Ion channel activity of influenza A virus M2 protein: characterization of the amantadine block. J Virol 67:5585–5594
42. Webster R, Cox N, Stöhr K (2002) WHO animal influenza manual. WHO/CDS/CSR/NCS
43. Webster RG, Shortridge KF, Kawaoka Y (1997) Influenza: interspecies transmission and emergence of new pandemics. FEMS Immunol Med Microbiol 18:275–279
44. Youk S, Lee DH, Killian ML, Pantin-Jackwood MJ, Swayne DE, Torchetti MK (2020) Highly pathogenic avian influenza A(H7N3) virus in poultry, United States, 2020. Emerg Infect Dis 26:2966–2969

45. Zanin M, Kocer ZA, Poulson RL, Gabbard JD, Howerth EW, Jones CA, Friedman K, Seiler J, Danner A, Kercher L, McBride R, Paulson JC, Wentworth DE, Krauss S, Tompkins SM, Stallknecht DE, Webster RG (2017) Potential for low-pathogenic avian H7 influenza A viruses to replicate and cause disease in a mammalian model. J Virol 91(3):e01934–16. https://doi.org/10.1128/JVI.01934-16. PMID: 27852855; PMCID: PMC5244340
46. Zhou A, Zhang J, Li H, Xu Q, Chen Y, Li B, Liu W, Su G, Ren X, Lao G, Luo B, Liao M, Qi W (2022) Combined insertion of basic and non-basic amino acids at hemagglutinin cleavage site of highly pathogenic H7N9 virus promotes replication and pathogenicity in chickens and mice. Virol Sin 37:38–47